Ultra-High-Sensitivity Temperature Sensor Using a Fiber Loop Mirror Based on a Water-Filled Asymmetric Two-Hole Fiber

Rodolfo Martínez-Manuel, Daniel A. May-Arrioja, Jesús Acevedo-Mijangos, René F. Domínguez-Cruz, Daniel López-Cortés, and Miguel Torres-Cisneros

***Abstract*—We present an ultra-high sensitivity fiber loop mirror temperature sensor based on an asymmetric two-hole fiber (ATHF) filled with distilled water. The design of the ATHF allows for larger interaction between the optical mode and the region with large induced birefringence. This enhanced interaction provides large changes in the sensing signal when the temperature is varied. The sensing signal can easily be tracked by following the change in the frequency of the interference signal as a function of the temperature, thus allowing for absolute temperature measurements. Experimental results show that the ATHF birefringence is modified from 1.18×10^{-5} to 3.33×10^{-4} when the temperature changes from 40 to 80 °C; generating, in terms of frequency, a sensitivity of 6×10^{-3}nm^{-1}/°C. In the case of very small temperature changes, where the wavelength shift is also small, simulations were performed using experimental parameters of the ATHF and an ultra-high sensitivity of 240 nm/°C was calculated. The sensitivity of the presented sensor can also be tuned by changing the liquid infiltrated into the fiber holes.**

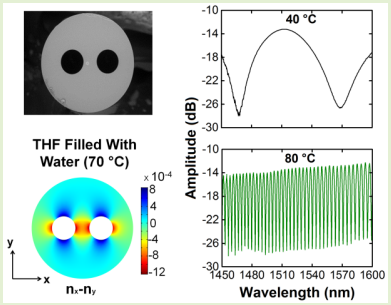

***Index Terms*— Fiber optic sensor, temperature fiber sensor, sagnac fiber sensor, two-hole fiber.**

I. Introduction

RECENTLY, the interest in developing temperature fiber sensors based on fiber loop mirror (FLM) has been increasing [1]–[7]. One of the key features of FLMs is related to the fact that they use a highly birefringent (Hi-Bi) fiber to generate the optical path difference in the fiber loop. As a result, the FLM temperature sensor configuration, compared to traditional interferometers such as Fabry-Perot, Michelson, and Mach-Zehnder, has the advantages of input polarization independence and the period of the interference spectra being dependent only on the length and birefringence value of the Hi-Bi fiber. Additionally, the FLM fiber sensor exhibits the same advantages as the traditional optical fiber sensors, such as immunity to electromagnetic interference, resistance to chemical corrosion, remote sensing, lightweight and small size [6].

Temperature sensors based on FLMs using commercial Hi-Bi fibers have widely been reported [6], [8], [9]. The internal birefringence of these fibers is commonly generated either by a geometrical effect of the fiber core or by the stress induced around the fiber core. Fiber sensors implemented using the Hi-Bi fiber based on geometrical effects have been reported to exhibit temperature sensitivities of -0.2 and -0.34 nm/°C, for e-core and D-type fibers respectively [6]. In contrast, those using Hi-Bi fibers based on stress effects, such as Panda and bow-tie fibers, have been reported to produce temperature sensitivities of -1.9 and -1.23 nm/°C respectively [6]. All of these reported temperature sensitivities are much higher than the 10 pm/°C reported for the popular fiber Bragg grating temperature sensors [10].

Manuscript received November 25, 2019; revised January 30, 2020 and February 14, 2020; accepted February 14, 2020. This work was supported in part by the Consejo Nacional de Ciencia y Tecnología under Grant CB2016-286368 and Grant CB2016-286629, in part by the Universidad Autónoma de Tamaulipas under Grant UAT-PFI-2018-CI-02, and in part by the Universidad de Guanajuato under Grant CIIC 72/2018. The work of Jesús Acevedo-Mijangos and Daniel López-Cortés was supported by CONACyT through the Postdoctoral Scholarship. The associate editor coordinating the review of this article and approving it for publication was Dr. Anuj K. Sharma. *(Corresponding author: Daniel A. May-Arrioja.)*

Rodolfo Martínez-Manuel, Daniel A. May-Arrioja, and Jesús Acevedo-Mijangos are with the Centro de Investigaciones en Óptica, Unidad Aguascalientes, Aguascalientes 20200, Mexico (e-mail: rodolfom@cio.mx; darrioja@cio.mx; jacevedo@cio.mx).

René F. Domínguez-Cruz is with the Electrical and Electronics Department, Universidad Autónoma de Tamaulipas, Reynosa 88779, Mexico (e-mail: rfdominguez@docentes.uat.edu.mx).

Daniel López-Cortés is with the Facultad de Ciencias en Física y Matemáticas, Universidad Autónoma de Chiapas, Tuxtla Gutiérrez 29050, Mexico (e-mail: lopezcdaniel@gmail.com).

Miguel Torres-Cisneros is with the Applied Physics Group, DICIS, University of Guanajuato, Salamanca 368850, Mexico (e-mail: torrescisneros@gmail.com).

This article has supplementary downloadable material available at http://ieeexplore.ieee.org, provided by the authors.

Digital Object Identifier 10.1109/JSEN.2020.2974889

In recent years, different configurations of FLMs using commercially available Hi-Bi fibers have been investigated in order to improve the sensitivity of FLM temperature sensors. In one configuration, two FLM interferometers were connected in a cascade configuration, with one implemented as a fixed signal interferometer and the other as the sliding part of a Vernier scale. For instance two cascaded FLM interferometers were employed to generate a temperature sensitivity of -13.36 nm/°C [3], and in another configuration that employed a combination of an FLM and a Fabry-Perot interferometer, a temperature sensitivity of -29 nm/°C [1] was reported. Although the sensitivity is improved, the use of specialty fibers provides new schemes that can improve the sensitivity of FLM temperature sensors by several orders of magnitude.

The development of photonic crystal fibers (PCF) has provided several advantages that were not available in conventional fibers. These include fiber mode shaping, high nonlinearities, dispersion and birefringence [11]. The high internal birefringence in PCFs is generated by a geometrical effect. Through the arrangement of microscopic air holes along the fiber length, it has been made possible to build temperature insensitive interferometers by using a polarization maintaining PCF in an FLM interferometer [12], [13]. In this configuration, the changes in temperature equally affect the silica core and cladding sections of the fiber, while leaving the air-holes sections unaffected, and hence the birefringence remains unchanged. However, in recent years, FLMs implementing PCFs have been reported as high-sensitivity temperature fiber sensors [2], [5], [14]. In order to modify the birefringence value of a Hi-Bi PCF, the PCF has side-holes that are filled with liquids such as alcohol and toluene, and metals such as indium, and the devices have reported temperature sensitivities of 6.1 nm/°C [14], 11 nm/°C [15] and -9 nm/°C [2]. The enhancement in temperature sensitivity of the fiber with liquid filled side-hole, is caused by the thermo-optic effect of the liquid sample; while in the metal-filled fiber configurations, the enhancement in temperature sensitivity comes from the thermal expansion coefficient of the metal.

It should be noted that the incorporation of side-holes is not exclusive to PCF, for they have been also implemented in standard single mode fibers (SMF). In fact, in contrast to those results reported in [2], [14], [15] that used PCF with side-holes, a specialty SMF fiber has been developed that contains only two holes [4], [5], [16]. This type of two-hole fiber is also simpler to manufacture as compared to the traditional PCFs. In [5], a two-hole birefringent fiber was filled with metal (indium) and configured as an FLM temperature sensor that recorded a temperature sensitivity of -6.3 nm/°K. In [4], a two-hole fiber in an FLM configuration was filled with alcohol and a temperature sensitivity of 86.8 pm/°C was obtained. Also, the rapid change in the birefringence of the two-hole fiber at the temperature of phase transition of the filler substance, water, salt water and metal, were studied in [16]. More recently, we have presented the implementation of a two-air-hole birefringent fiber in an FLM configuration, where a temperature sensitivity of 2.21 nm/°C was reported [17].

Regardless of the type of birefringent fiber or the implemented configuration, among all the reported systems using FLMs as a temperature sensor, the highest achieved sensitivity was -29 nm/°C [1]. In addition, since the achieved wavelength shifts are relatively small, the changes in temperature are measured by following a resonant-dip in the spectral response of the FLM temperature sensor.

In this work, we report the implementation of a fiber loop mirror temperature sensor based on an asymmetric two-hole fiber (ATHF), filled with distilled water, which exhibits an extremely temperature sensitivity. The key component is the ATHF, which provides a large overlap between the optical mode and the region with the highest induced birefringence, and therefore the birefringence is strongly affected when the ATHF is heated. In addition to the large wavelength shift of the spectrum due to the temperature dependent birefringence, there is also a significant change in the fringe spacing of the interference signal. The latter effect allowed for the processing of the sensing signal in the frequency space, and therefore reporting the changes in temperature in terms of the signal frequency. After calibration, the recording of the interference signal frequency can lead to absolute measurements of temperature. A sensitivity of $6\times\ 10^{-3}$ nm^{-1}/°C was obtained for coarse temperature changes from 40 to 80 °C. This is different from previously reported FLM temperature sensing systems, which track a resonant dip in the interference spectrum; instead, the Fourier transform of the measured interference spectrum is used to determine the temperature value. For temperature changes of a fraction of a degree Celsius, the wavelength shift of a resonant dip can be monitored, and our results demonstrate that the temperature sensor has a sensitivity of 240 nm/°C. To the best of our knowledge, this is the highest sensitivity reported so far for temperature sensors using the FLM configuration.

II. Asymmetric Two-Hole Fiber (ATHF) Design

The ATHF was designed to enhance the induced birefringence obtained from heating the ATHF when the holes are filled with liquid. In this scenario, we have two potential contributions to the induced birefringence. The first one is related to the thermal expansion of the liquid into the holes which induces birefringence due to the stress-optic effect, and the second one is related to the refractive index changes of the liquid and silica via thermo-optic effects. We should keep in mind that in this kind of optical fiber that includes two holes, any change to the holes diameter, core diameter, separation between the holes, and position of the holes will slightly modify the sensitivity of the sensor [18]. Therefore, we fixed some parameters, such as the diameter of the holes and fiber core, the separation between holes, and the only variable left was the position of the holes with respect to the fiber core. An external diameter of 125 μm was used for the optical fiber which facilitates splicing to standard SMF, and the diameter of the holes is set to 29 μm which is within the average diameter that has been used in previous works [4], [16], [18]–[20]. The separation between the holes is set to 17 μm and they are symmetrically positioned with respect to the optical fiber axes as shown in Fig. 1 (a) and (b).

The optimum ATHF parameters were obtained via Finite Element Method (FEM) simulations using the commercial software COMSOL Multiphysics. The simulation was performed using 2D analysis, selecting solid mechanics (plane

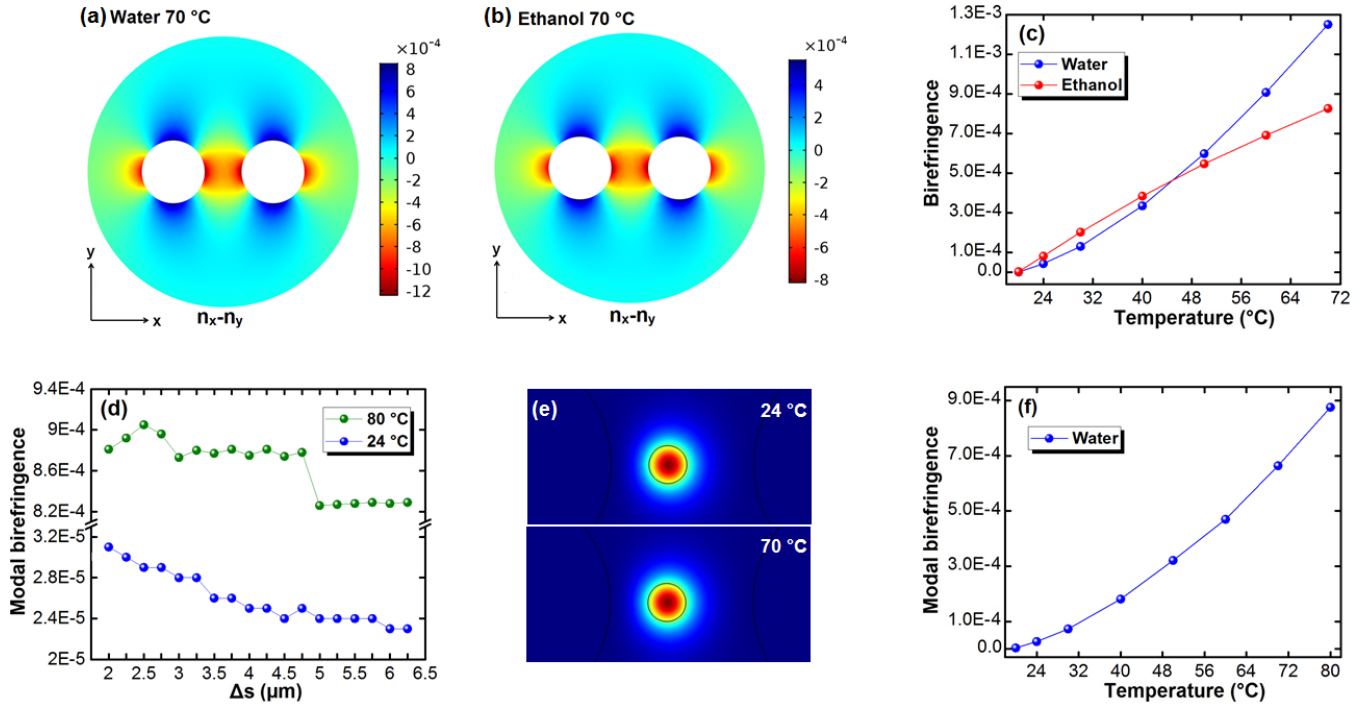

Fig. 1. Induced birefringence distribution in the two-hole fiber at 70 °C for (a) Water and (b) Ethanol, and (c) Maximum birefringence value as a function of temperature for water and ethanol. (d) Modal birefringence as a function of the separation (Δs) between the inner edge of the left hole to the edge of the fiber core at 24 °C and 80 °C, (e) Optical modes with ethanol infiltrated into the holes at 24 °C and 70 °C, and (f) Modal birefringence of the ATHF design as a function of temperature using water as the filling liquid.

stress) from the structural mechanics module as well as electromagnetics wave (frequency domain) from the optics module. The optical and material properties used in the FEM simulations are shown in Table 1. During simulations the mesh used was free triangular with fine size and the reference temperature was set to 20°C. Any other parameter used the default values provided by COMSOL.

In the solid mechanics section we ran a stationary study that provides the principal stresses (σ_x, σ_y and σ_z) in the ATHF. Using this data and equation 1, we can estimate the refractive index change in the ATHF as a result of the induced stress. Here n_0 is the refractive index of the unstressed material, and $C_1 = 0.65\times10^{-12}m^2/\text{N}$ and $C_2 = 4.2\times10^{-12}m^2/\text{N}$ are the elasto-optic coefficients [16].

In the electromagnetics wave (frequency domain) we have to choose the diagonal option in the real refractive index in order to incorporate the refractive changes (n_x, n_y and n_z). A mode analysis study is then performed to calculate the effective refractive indexes for the TE and TM modes of the ATHF. Using these effective indexes we then calculate the modal birefringence using $B = n_{eff}TM - n_{eff}TE$ [25].

$$\begin{aligned} n_x &= n_0 - C_1\sigma_x - C_2\left(\sigma_y + \sigma_z\right) \\ n_y &= n_0 - C_1\sigma_y - C_2(\sigma_x + \sigma_z) \\ n_z &= n_0 - C_1\sigma_z - C_2(\sigma_x + \sigma_y) \end{aligned} \quad (1)$$

Firstly we have to choose the liquid infiltrated into the holes from a variety of liquids that have been previously reported [4], [7], [16], [20], [26], [27]. Among such liquids water and alcohol have been widely used because they exhibit a large

TABLE I
OPTICAL AND MATERIALS PROPERTIES USED IN FEM ANALYSIS

Material	Properties				
	n_0 [a] at 1550 nm, 20°C	TOC [a]	E [a] (GPa)	α [a] (1/°C)	v [a]
Core	1.4493	1.18×10^{-5}	Corning 7940 [b]	9.4×10^{-7}	Corning 7940 [b]
Cladding	1.444	1.18×10^{-5}	Corning 7940 [b]	5.4×10^{-7}	Corning 7940 [b]
Alcohol	1.352	-3.38×10^{-4}	[21]	[22]	0.49
Water	1.318	-1.24×10^{-4}	[23]	[22,24]	0.49

[a] n_0= refractive index, TOC= Thermo-optic coefficient, E= Young´s modulus, α = Thermal expansion coefficient and v= Poisson´s ratio.
[b] Corning 7940 (fused silica) is a material in the library of COMSOL Multiphysics.

thermal expansion coefficient, and this is correlated with the fact that a larger stress will be induced in the two-hole fiber (THF) due to the liquid expansion. Based on the above we perform simulations with both liquids filling the THF and select the one that provides larger temperature sensitivity. As shown in Fig. 1 (a) and (b), when the THF filled either with water or alcohol is heated up to 70°C, the induced birefringence is maximum at the edges of the holes along the horizontal direction regardless of the liquid. Therefore by plotting the maximum birefringence value at the inner edge of either hole we can determine which liquid induces the largest birefringence. As shown in Fig. 1 (c), the largest induced birefringence as a function of temperature is achieved with

water, which in turn provides larger temperature sensitivity. Water is then selected as the filling liquid in the following simulations.

Since maximum birefringence is induced at the edge of the holes, a small fiber core with a diameter of 4.5 μm is considered in order to maximize the induced birefringence change as a function of temperature experienced by the optical mode - i.e., lowest induced birefringence at 24 °C and maximum induced birefringence at 80 °C. The fiber core is centered along the optical fiber axes, in order to facilitate splicing to SMF, and the holes are shifted along the horizontal direction to find the optimum separation (Δs) between the inner edge of one of the holes to the edge of the fiber core. We start by placing the inner edge of the left hole at a distance of $\Delta s = 2$ μm with respect to the edge of the fiber core, and the induced modal birefringence is calculated at 24 °C and 80 °C. As shown in Fig. 1(d) we continue increasing the value of Δs in steps of 250 nm and the induced modal birefringence is calculated at both temperatures. As shown in Fig. 1(d), the maximum increment in the induced birefringence, as the temperature is increased, is not when the separation $\Delta s = 2$ μm but when we have a separation of $\Delta s = 4.5$ μm between the edges of the left hole and fiber core.

In order to evaluate the impact of thermo-optic effects, the fiber core is positioned along the optical fiber axes and the holes are asymmetrically positioned with a separation between the edges of the left hole and fiber core of 4.5 μm. The thermo-optically induced birefringence of this ATHF is calculated by using ethanol instead of water because ethanol exhibits a higher refractive index that could more easily modify the fiber birefringence. As shown in Fig. 1 (e), the mode is practically unchanged when the temperature is raised from room temperature to 70 °C. In fact, the induced modal birefringence resulting from thermo-optic contribution is zero according to our simulations. Based on the simulations the optimum ATHF parameters should have a separation between edge of the core and the inner edge of the holes of 4.5 μm and 8 μm, taking into account a core diameter of 4.5 μm, and holes diameters of 29 μm with a hole to hole separation of 17 μm.

Finally, using this ATHF design, we perform simulations to estimate the modal birefringence as a function of temperature using water as the filling liquid. As shown in Fig. 1 (f), although the behavior is quite similar when the birefringence was measured at the maximum value (edge of the hole), the maximum modal birefringence is slightly lower because the mode initially overlaps with regions of lower birefringence. Nevertheless, this ATHF design allows for the maximum increment on the induced birefringence as the temperature is increased, which also provides the largest sensitivity. The total birefringence changes from 2.7×10^{-5} at 24 °C to 8.76×10^{-4} at 80 °C, which is significantly larger as compared to previous reports.

III. Experimental Setup

The ATHF was manufactured at ACREO Fiberlab (Kista, Sweden), and a cross-section of the ATHF is shown in Figs. 2 (a) and (b). The outer diameter of the fiber is 125 μm,

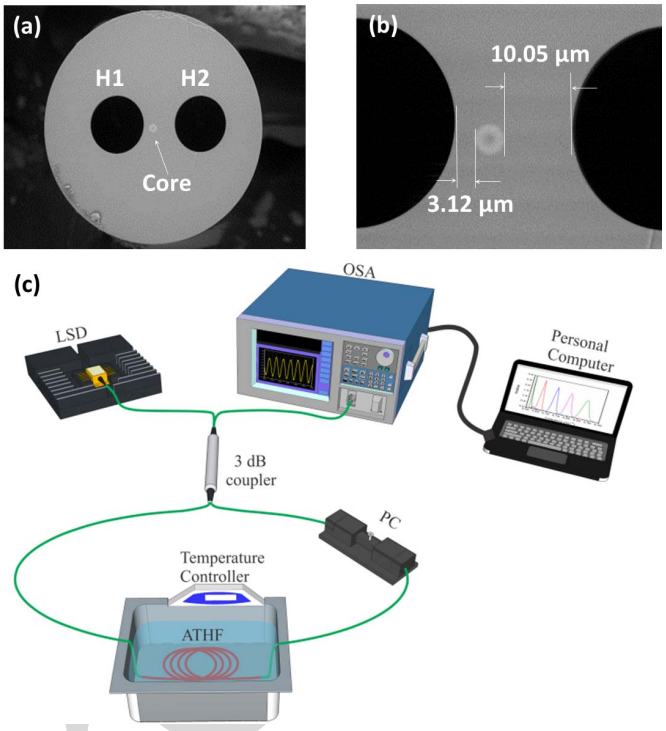

Fig. 2. (a) Cross section image of the ATHF, (b) Zoomed image between the holes of the ATHF, and (c) Experimental setup used to test the water filled-ATHF as a temperature sensor.

which is fully compatible with SMF, and the core diameter is 4.2 μm. The two holes are asymmetrically located into the fiber: the nearest hole to the fiber core has a diameter of H1 = 29.12 μm and its inner edge to the edge of the fiber core has a separation of 3.12 μm, while the other hole has a diameter of H2 = 27.91 μm and its inner edge to the edge of the fiber core has a separation of 10.05 μm. In general, the ATHF is slightly similar to previously reported THF since it is basically an SMF with two holes running along the fiber. Nevertheless, the fact that the holes are asymmetrically positioned with respect to the center of the core, allows us to place the edge of one of the holes in very close proximity to the edge of the core. The proximity of the hole to the core provides a higher interaction between the optical mode and the region of higher induced birefringence, such that changes on the surrounding temperature will induce larger birefringence changes in the ATHF. In addition, the fact that the other hole has enough separation from the core provides a thicker section of material between the holes that reduces the complexity during the fabrication of the ATHF. The dimensions measured in Fig. 2 (a) and (b) correspond to the best match of our experimental ATHF with respect to the simulated design parameters.

The temperature sensor structure consists of a 2 m segment of ATHF filled with water and spliced between two pieces of SMF in an FLM configuration. Prior to splicing the fibers, the process to fill the ATHF with water was as follows: one tip of the ATHF was submerged into distilled water contained in a glass vial and due to the capillary action the liquid is introduced along the two holes of the fiber. On the other

end of the ATHF low vacuum was applied to accelerate the process and flow the liquid to avoid the formation of air gaps or bubbles. Subsequently, the two ends of the filled-ATHF were warmed up to remove the liquid from the tips, in order to get enough space for splicing the SMF fibers and enclose the liquid inside the structure. In our experiments, a distance of 7 mm between the liquid and the tip of the fiber was considered, which is enough to perform the splicing procedure and to induce negligible effects in the spectral response due to expansion of the liquid as the ATHF is heated. A standard fusion splicer (Fujikura model 70S) and a conventional program for SMF splicing were employed for this purpose.

The sensor characterization was performed using the experimental setup shown in Fig. 2 (c). The FLM was fabricated using a 2 × 2.3-dB coupler where the output ports are connected to the filled-ATHF segment (length L = 2 m) through a mechanical polarization controller (PC). A superluminescent diode (SLD), emitting from 1440 nm to 1620 nm and centered at 1530 nm, was used as the optical source and connected to one of the input ports. The other input port is used to monitor the transmitted spectrum using an Optical Spectrum Analyzer (OSA). The temperature was controlled by immersing the ATHF segment in an ultrasonic bath filled with water which incorporates a temperature controller with a resolution of 1 °C.

IV. Results and Discussion

The temperature measurements were performed by acquiring the transmitted spectrum as a function of the applied temperature with steps of 5 °C in the range from 40 °C to 80 °C. The lowest temperature is set at 40 °C in order to visualize at least two valleys in the interference pattern within the wavelength range of the SLD, which is a requirement to estimate the birefringence value at a given temperature. The spectral response of the sensor for four different temperatures, 40 °C, 55 °C, 65 °C and 80 °C, is presented in Fig. 3, where an abrupt reduction of the fringes period can be easily observed as the temperature is increased, which is correlated with a significant increment in the birefringence of the fiber. We should note that the wavelength shift in the interference pattern as a function of temperature was so large, that we have to wait for full temperature stabilization in order to acquire a stable transmitted spectrum. This ultra-high sensitivity will be analyzed in detail at the end of this section.

The mechanism behind such large birefringence change is related to the different parameters of the ATHF. Firstly, the thermal expansion of the infiltrated liquid induces birefringence changes in the ATHF, with their maximum values at the edges of the holes. Secondly, the core is close to the inner edge of the hole and the diameter of the ATHF is smaller (4.2 μm) than the standard SMF core diameter, which forces the optical mode to overlap the region with larger induced birefringence and thus its birefringence is also increased. The reduction of the fringe spacing is then expected, as dictated from the well-known birefringence equation: $\Delta n = \lambda_c^2 / \Delta\lambda L$; where Δn is the birefringence, λc is the center wavelength of the spectrum, $\Delta\lambda$ is the period of the interference fringes, and L is the length of the filled-ATHF.

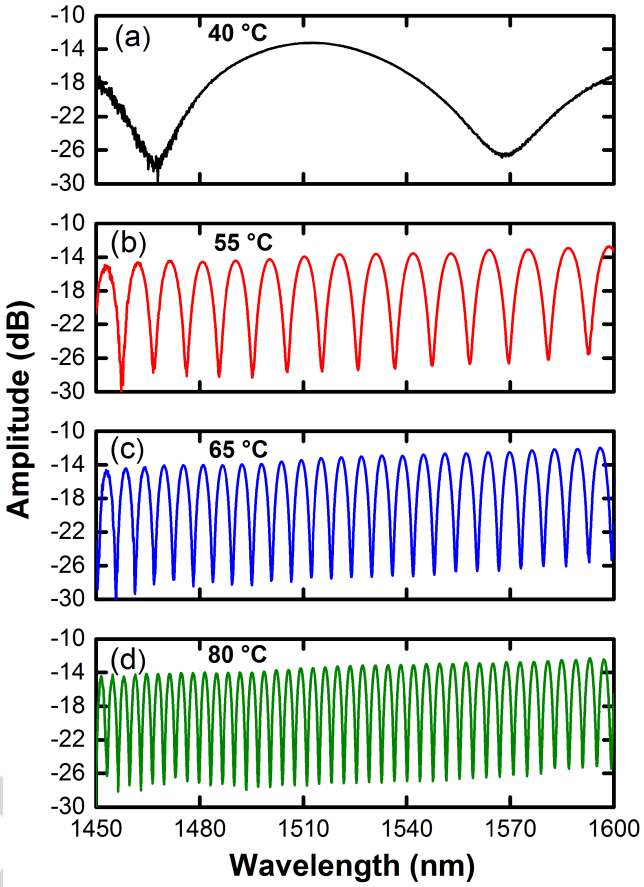

Fig. 3. Transmission spectra of the FLM fabricated with the filled ATHF at temperatures of (a) 40 °C, (b) 55 °C, (c) 65 °C, and (d) 80 °C.

As shown in Fig. 3, the fringe spacing $\Delta\lambda$ significatively changed as the temperature is increased, going from 101 nm to 3.35 nm for 40 and 80 °C respectively. Using the birefringence equation mentioned before, we can estimate from the fringe spacing the corresponding birefringence values as a function of the applied temperature. As shown in Fig. 4, the results indicate an excellent linear approximation with a temperature sensitivity of 7.8713×10^{-6}/°C. In fact, birefringence values of 1.1815×10^{-5} for 40 °C and 3.3367×10^{-4} for 80 °C were estimated, which corresponds to a remarkable increment of the birefringence of more than 28 times from 40 °C to 80 °C.

Based on the above results we must consider that small changes in temperature are correlated with large changes of the interference spectrum from the FLM, for instance an increment of 1 °C generates a huge wavelength shift of 240 nm (i.e. sensitivity of 240 nm/°C), which makes the system suitable for ultra-sensitive temperature measurement applications. Then, in our experiment, taking into consideration the large change in the fringe spacing as a result of temperature variations, the spectrum was Fourier transformed to obtain the frequency response as a function of temperature and facilitates reading of the sensor response. In order to reduce the spreading of the frequency components of each spectrum, a Hanning window was applied to the spectra before converting to frequency space, as shown in Fig. 5(a) for an applied temperature of 65 °C.

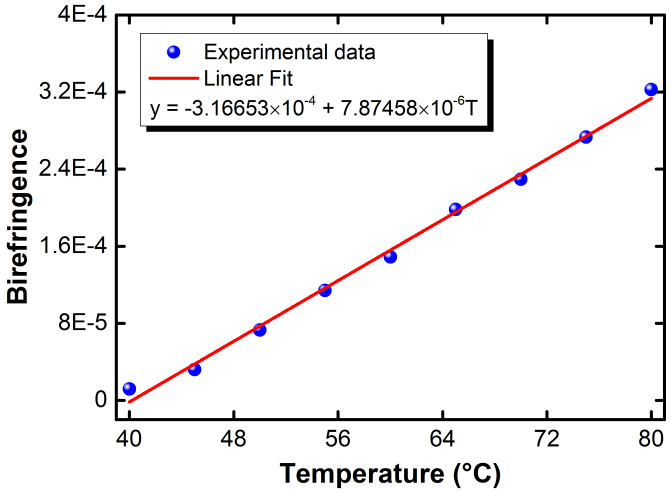

Fig. 4. Birefringence value as a function of the applied temperature.

The fringes frequency for each temperature measurement is presented in Fig. 5(b). As can be seen, the equidistant change in temperature, 5 °C step, generates an equidistant change in frequency. Due to the limited spectral range of 180 nm of the optical source implemented in our setup, only a few cycles can be recorded for the spectrum generated at 40 °C and 45 °C, as shown in Fig. 3(a) for the spectrum at 40 °C. Therefore, frequencies for these temperature values are close to the DC component in the frequency spectrum and are not displayed in Fig. 5(b). However, this drawback can be easily overcome by the implementation of an optical source with a broader spectrum such as a supercontinuum laser. The implementation of such a broader optical source will also contribute to significantly narrow the frequency response shown in Fig. 5(b).

In Fig. 6, the frequency components as a function of the applied temperature values are presented, and a linear response can be observed within the range of temperature measurements. Since no phase or amplitude is tracked in the measurement process, once the sensor is calibrated, the fringes frequency obtained for each applied temperature is repeatable, allowing for absolute measurements. In terms of frequency, a sensitivity of 6×10^{-3} nm^{-1}/°C is obtained. The repeatability of the proposed sensor was measured using the following procedure: first, the FLM was introduced into the ultrasonic bath (set at 60 °C) and a measurement was taken, then, the FLM was removed from the ultrasonic bath, wait five minutes to expose it at room temperature, and again, the FLM was introduced into the bath to take another measurement. This process was repeated 20 times to obtain a repeatability in the frequency component corresponding to 1 °C.

Considering the ultra-high sensitivity of the temperature sensor, it is important to investigate its response to very small temperature increments on the order of 0.01 °C. Taking into account that our temperature controller cannot provide such small temperature increments, we performed a simulation to present the response of the sensor to temperature changes in the order of a fraction of a degree Celsius; where we use the change of birefringence as a function of temperature

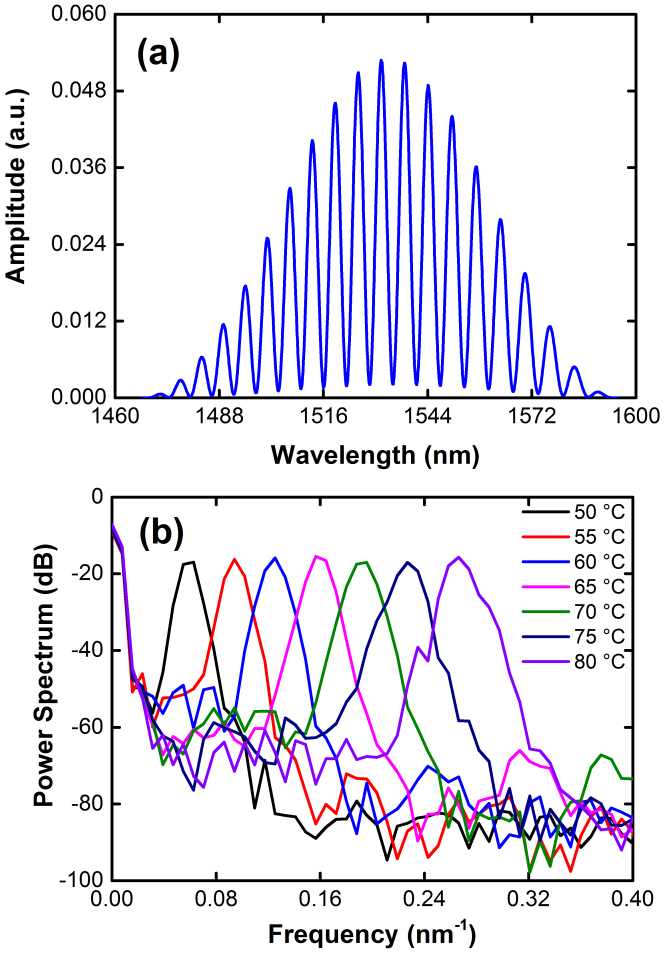

Fig. 5. (a) The transmission spectrum of the FLM at 65 °C, with a Hanning window applied to it; (b) Frequency spectrum of the sensing signal for different temperature values.

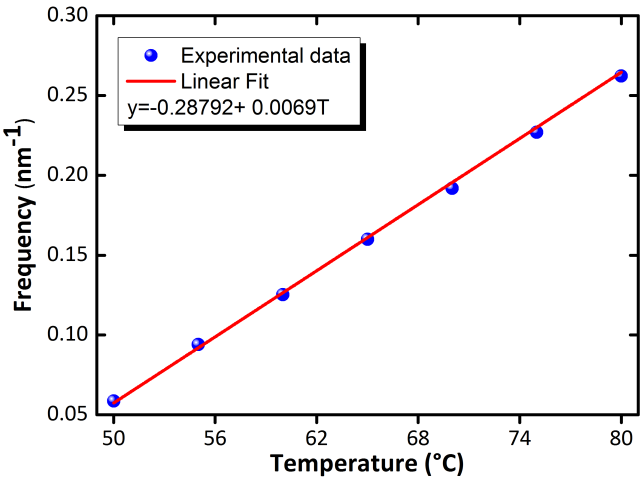

Fig. 6. Spatial frequency response at different temperatures.

obtained from the experiments results in Fig. 4. In order to do so, we performed simulations of the proposed sensor by implementing the well-known equation [6], [12], for the

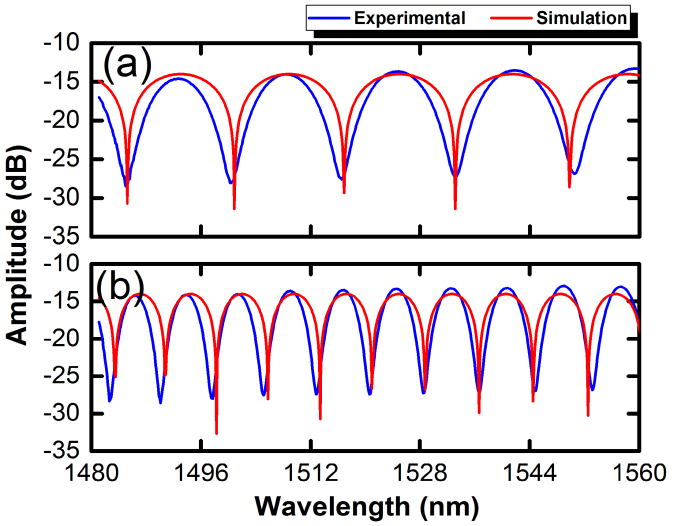

Fig. 7. (a) Transmission spectrum of the temperature sensor, experiment and simulation, at 50 °C (b) The sensor spectrum, experiment and simulation, at 60 °C.

transmitted spectrum of the FLM,

$$trans\,(\lambda) = sin^2\left[(\pi L/\lambda)\,(\Delta n\,(T_0) + (T - T_0)\,d\Delta n/dT)\right], \tag{2}$$

where L is the length of the ATHF, λ is the light wavelength, Δn is the ATHF group index birefringence, T_0 is the reference temperature, T is the temperature to be measured, and $d\Delta n/dT$ is the temperature sensitivity as obtained from the experiments. Simulations were performed using data obtained from the experimental results, such as the birefringence and sensitivity at the measured temperature. As a first step we verified that the simulations are in agreement with the experimental results previously obtained based on larger temperature increments. As shown in Fig. 7(a) and 7(b), we present the transmitted spectrum when the fiber is subjected to 50 °C and 60 °C, respectively, showing an excellent agreement between experiment and simulation. This effectively guarantees that our simulations for small temperature increments will be accurate. We should note that there is a difference between the linewidth of the experimental fringes and the theoretical values. We believe that this linewidth difference might be related to slight birefringence variations along our experimental ATHF, which tends to broaden its spectral response. Therefore, we numerically calculated the transmitted spectral response of the sensor for temperature increments from 0.01 °C to 0.06 °C, in steps of 0.01 °C, for an initial temperature of 45 °C. As shown in Fig. 8(a) and 8(b) we can easily observe a spectral shift of approximately 2.4 nm for a temperature increment of 0.01 °C. The simulation corroborates the ultra-high sensitivity of the sensor since any small change in temperature generates a considerable spectral shift. Therefore, for applications where very small temperature changes are required and considering the implementation of an OSA with a modest resolution of 0.1 nm, our system will perform with a resolution of 4×10^{-4}°C. If we consider an OSA with higher resolution, as in the case of a research grade OSA with a resolution of 0.06 nm, an even higher temperature resolution can be achieved.

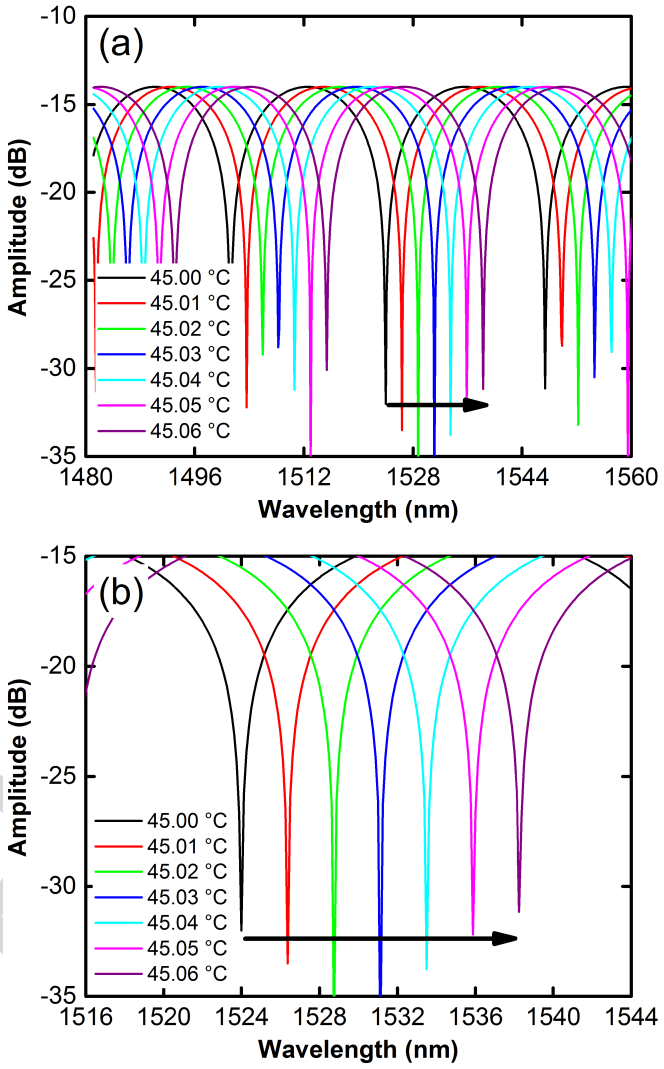

Fig. 8. (a) Simulation of the transmission spectrum of the sensor with a temperature change in steps of 0.01 °C (b) zooming in (a) to show the 14.4 nm red-shift in the resonant dip after a small change in temperature of 0.06 °C.

Considering that our temperature controller cannot provide such small temperature increments, we decided to perform a much simpler experiment to show the large sensitivity of the sensor. As shown in visualization 1, the ATHF in the FLM is placed inside a plastic container to minimize fluctuation due to variations of the room temperature. Despite this approach, within the first 5 seconds of visualization 1, we can observe slight wavelength shifting due to temperature fluctuations in the room. When we start approaching the sensor with our bare hands, we can observe a large spectral shift with a maximum value of 28 nm, even when we never touch the ATHF. Afterwards, we start approaching a soldering iron with a set temperature of 125 °C, and we can observe a spectral shift even when the soldering iron has not appeared in the video. When the soldering iron is very close to the ATHF, again without touching the ATHF, the spectral shifting is significantly large (see visualization 1). The response time can also be estimated from visualization 1 and is estimated to be within a second.

Compared to previously reported FLM based temperature sensors, the presented system exhibits ultra-high temperature sensitivity and the design of the ATHF is key to obtain this performance. We should also highlight that the holes diameter is large enough to facilitate the liquid filling process. In addition, the fact that one of the holes is quite close to the ATHF core also provides a more significant influence of the induced birefringence. The size of the side holes also opens the possibility to implement the system with other liquids, depending on the application, for example, to make the system more or less sensitive and/or being able to perform measurements in a more significant range.

V. Conclusions

An ultra-high sensitive temperature fiber sensor was proposed and experimentally demonstrated. In this sensor, we use a special ATHF which is basically an SMF with two adjacent holes running along the optical fiber. The holes are asymmetrically positioned in such a way that one of the holes is significantly close to the ATHF core, which also induces birefringence in the ATHF. By filling the holes with distilled water we allow the fiber to be highly sensitive to temperature fluctuations, which in turn modifies the birefringence of the ATHF as the temperature is changed. As a result, the sensor exhibits an ultra-high sensitivity and the changes in temperature generate significant changes in the period of the sensor transmission spectrum, which allow us to Fourier transform the sensor signal and identify the changes in temperature as changes in the frequency of the spectrum. Experimental results show that the ATHF birefringence is modified from 1.18×10^{-5} to 3.33×10^{-4} for temperature changes from 40 to 80 °C, respectively. With such large changes in birefringence the sensor exhibits a sensitivity, in terms of frequency, of 6×10^{-3} nm^{-1}/°C. Also, for very small temperature changes where the resonant dip wavelength shift can be monitored, the temperature sensor response is correlated with an ultra-high sensitivity of 240 nm/°C. Considering a low performance OSA of 0.1 nm resolution, a temperature sensor resolution of 4×10^{-4}°C is estimated, which could be higher if we consider a research grade OSA with even higher resolution. We should highlight that by changing the filling-liquid we can also control the sensitivity of the sensor, which is ideal for specific applications.

Acknowledgment

The authors would like to thank Dr. W. Margulis from ACREO Fiberlabs (RISE ACREO) for providing the ATHF used in this experiments. They would also like to thank Guanajuato University-CONACYT National Laboratory for SEM analysis.

References

[1] Y. Yang *et al.*, "Sensitivity-enhanced temperature sensor by hybrid cascaded configuration of a sagnac loop and a F-P cavity," *Opt. Express*, vol. 25, no. 26, pp. 3683–3685, Dec. 2017.

[2] E. Reyes-Vera, C. M. B. Cordeiro, and P. Torres, "Highly sensitive temperature sensor using a sagnac loop interferometer based on a side-hole photonic crystal fiber filled with metal," *Appl. Opt.*, vol. 56, no. 2, pp. 156–162, Jan. 2017.

[3] L.-Y. Shao *et al.*, "Sensitivity-enhanced temperature sensor with cascaded fiber optic sagnac interferometers based on Vernier-effect," *Opt. Commun.*, vol. 336, pp. 73–76, Feb. 2015.

[4] Y. Xin, X. Dong, Q. Meng, F. Qi, and C.-L. Zhao, "Alcohol-filled side-hole fiber sagnac interferometer for temperature measurement," *Sens. Actuators A, Phys.*, vol. 193, pp. 182–185, Apr. 2013.

[5] B. H. Kim, S. H. Lee, A. Lin, C.-L. Lee, J. Lee, and W.-T. Han, "Large temperature sensitivity of sagnac loop interferometer based on the birefringent holey fiber filled with metal indium," *Opt. Express*, vol. 17, no. 3, pp. 1789–1794, Jan. 2009.

[6] O. Frazão, J. Baptista, and J. Santos, "Recent advances in high-birefringence fiber loop mirror sensors," *Sensors*, vol. 7, no. 11, pp. 2970–2983, Nov. 2007.

[7] Y. Cui, P. P. Shum, D. J. J. Hu, G. Wang, G. Humbert, and X.-Q. Dinh, "Temperature sensor by using selectively filled photonic crystal fiber sagnac interferometer," *IEEE Photon. J.*, vol. 4, no. 5, pp. 1801–1808, Oct. 2012.

[8] Y. Liu *et al.*, "High-birefringence fiber loop mirrors and their applications as sensors," *Appl. Opt.*, vol. 44, no. 12, p. 2382, Apr. 2005.

[9] J. Zhang *et al.*, "Highly sensitive temperature sensor using PANDA fiber sagnac interferometer," *J. Lightw. Technol.*, vol. 29, no. 24, pp. 3640–3644, Dec.15, 2011.

[10] K. O. Hill and G. Meltz, "Fiber Bragg grating technology fundamentals and overview," *J. Lightw. Technol.*, vol. 15, no. 8, pp. 1263–1276, Aug. 1997.

[11] J. C. Knight, "Photonic crystal fibres," *Nature*, vol. 424, no. 6950, pp. 847–851, 2003.

[12] D.-H. Kim and J. U. Kang, "Sagnac loop interferometer based on polarization maintaining photonic crystal fiber with reduced temperature sensitivity," *Opt. Express*, vol. 12, no. 19, pp. 4490–4495, 2004.

[13] C.-L. Zhao, X. Yang, C. Lu, W. Jin, and M. S. Demokan, "Temperature-insensitive interferometer using a highly birefringent photonic crystal fiber loop mirror," *IEEE Photon. Technol. Lett.*, vol. 16, no. 11, pp. 2535–2537, Nov. 18. 2004.

[14] W. Qian *et al.*, "High-sensitivity temperature sensor based on an alcohol-filled photonic crystal fiber loop mirror," *Opt. Lett.*, vol. 36, no. 9, pp. 1548–1550, Apr. 2011.

[15] Y. E. Monfared, C. Liang, R. Khosravi, B. Kacerovska, and S. Yang, "Selectively toluene-filled photonic crystal fiber sagnac interferometer with high sensitivity for temperature sensing applications," *Results Phys.*, vol. 13, Jun. 2019, Art. no. 102297.

[16] J. Jason, P. Rugeland, O. Tarasenko, W. Margulis, and H.-E. Nilsson, "Temperature characteristics of the birefringence properties of filled side-hole fibers," *Appl. Opt.*, vol. 52, no. 21, pp. 5208–5215, Jul. 2013.

[17] R. Domínguez-Cruz, D. A. May-Arrioja, R. Martínez-Manuel, and D. Lopez-Cortes, "Temperature sensor based on an asymmetric two-hole fiber using a Sagnac interferometer," *J. Sensors*, vol. 2018, Feb. 2018, Art. no. 7595106.

[18] Z. Li, C. Sun, Y. Hu, H. Yang, and X. Zhang, "Study on the birefringence of the circular-core side hole fiber," *Proc. SPIE Adv. Sensor Syst. Appl.*, vol. 5634, pp. 478–480, Feb. 2005.

[19] S. Tanaka, K. Yoshida, S. Kinugasa, and Y. Ohtsuka, "Birefringent side-hole fiber for use in strain sensor," *Opt. Rev.*, vol. 4, no. 1, pp. A92–A95, Jan. 1997.

[20] Q. Zhang, L. Hu, Y. Qi, G. Liu, N. Ianno, and M. Han, "Fiber-optic refractometer based on a phase-shifted fiber Bragg grating on a side-hole fiber," *Opt. Express*, vol. 23, no. 13, pp. 16750–16759, Jun. 2015.

[21] eFunda. (2020). *Properties of Ethanol Alcohol*. [Online]. Available: https://www.efunda.com/materials/common_matl/show_liquid.cfm?MatlName=AlcoholEthanol

[22] A. I. Dragan, D. J. Russell, and P. L. Privalov, "DNA hydration studied by pressure perturbation scanning microcalorimetry," *Biopolymers*, vol. 91, no. 1, pp. 95–101, Jan. 2009.

[23] D. A. Chin, *Water-Quality Engineering in Natural Systems*. Hoboken, NJ, USA: Wiley, 2006, p. 537.

[24] G. Elert. (2020). *The Physics Hypertextbook: Thermal Expansion*. [Online]. Available: https://physics.info/expansion/

[25] H. P. Schriemer and M. Cada, "Modal birefringence and power density distribution in strained buried-core square waveguides," *IEEE J. Quantum Electron.*, vol. 40, no. 8, pp. 1131–1139, Aug. 2004.

[26] X. C. Yang, Y. Lu, B. L. Liu, and J. Q. Yao, "Temperature sensor based on photonic crystal fiber filled with liquid and silver nanowires," *IEEE Photon. J.*, vol. 8, no. 3, Jun. 2016. Art. no. 6803309.

[27] R. Wang *et al.*, "A reflective photonic crystal fiber temperature sensor probe based on infiltration with liquid mixtures," *Sensors*, vol. 13, no. 6, pp. 7916–7925, Jun. 2013.

Rodolfo Martínez-Manuel received the M.Sc. degree and the Ph.D. degree in optics from the Ensenada Center for Scientific Research and Higher Education (CICESE), Mexico, in 2004 and 2008, respectively. In 2009, he joined the Photonics Research Group, University of Johannesburg, South Africa, where he was the Head from 2012 to 2014. In 2015, he joined the Centro de Investigaciones en Óptica (CIO), Unidad Aguascalientes, Mexico, as a Research Scientist. His research interests are algorithm design for signal processing in sensor systems, research and development of fiber sensor systems, and development of fiber lasers for fiber sensors application.

Daniel A. May-Arrioja received the Ph.D. degree in optics from CREOL, The College of Optics and Photonics, University of Central Florida, Orlando, FL, USA, in 2006. His current research interests include integrated photonics and fiber-optic devices with applications to lasers, sensors and biosensors, and microelectromechanical systems. In 2015, he joined the Centro de Investigaciones en Óptica (CIO), Unidad Aguascalientes.

Jesús Acevedo-Mijangos received the M.S. degree in micro and nanosystems from the Micro and Nanotechnology Research Center, Universidad Veracruzana, Boca del Río, Veracruz, Mexico, in 2012, and the Ph.D. degree in electrical engineering from the Centro de Investigación y Estudios Avanzados del Instituto Politécnico Nacional (CINVESTAV-IPN), Zapopan, Jalisco, Mexico, in 2017. He currently holds a postdoctoral position at the Centro de Investigaciones en Óptica A. C., Aguascalientes, Aguascalientes, Mexico. His research interests include fabrication and design of micro-electromechanical systems (MEMS), design and analysis of microstructured optical fiber, and plasmonic devices.

René F. Domínguez-Cruz received the bachelor's degree in physics from Universidad Veracruzana and the M.Sc. and Ph.D. degrees in optics from the National Institute of Astrophysics, Optics and Electronics (INAOE) in 1998 and 2002, respectively. He is a full-time Professor with the Electrical and Electronic Department, Autonomous University of Tamaulipas (UAT), Tamaulipas, Mexico. He is also a invited Reviewer of the IEEE SENSORS JOURNAL and *Microwave and Optical Technology Letters*. His research interests include non-linear optics effects in materials, optical fiber sensors, and novel micro-structured waveguides, where he has been coauthoring articles in journals and international conferences.

Daniel López-Cortés received the B.Sc. degree in electronics from the Universidad Autónoma de Puebla, Mexico, in 2002, and the M.Sc. and Ph.D. degrees in optics from the National Institute of Astrophysics, Optics and Electronics, Puebla, Mexico, in 2007 and 2012, respectively. He is currently a Research Associate with the Universidad Autónoma de Chiapas, Tuxtla Gutiérrez, Mexico. His research interests include fabrication and applications of microstructured optical fibers, fiber-optics sensors, and photonics application with two-dimensional materials.

Miguel Torres-Cisneros received the Ph.D. degree in physics (nonlinear optics) from the Instituto Nacional de Astrofísica, Óptica y Electrónica, Puebla, Mexico, in 1997. He is currently a member of the Applied Physics Group and a Researcher with the Electronics Department, College of Engineering, University of Guanajuato. His current research interests include optical fiber sensors and their applications.